Received: 31 March 2020 | Revised: 21 August 2020 | Accepted: 24 August 2020

IET Power Electronics

DOI: 10.1049/pel2.12030

The Institution of Engineering and Technology WILEY

ORIGINAL RESEARCH PAPER

First self-resonant frequency of power inductors based on approximated corrected stray capacitances

Ignacio Lope[1,2] | **Claudio Carretero**[1] | **Jesus Acero**[3]

[1] Department of Applied Physics, University of Zaragoza, Zaragoza, Spain

[2] BSH Home Appliances Group, Zaragoza, Spain

[3] Department of Electronic Engineering and Communications, University of Zaragoza, Zaragoza, Spain

Correspondence
Claudio Carretero, Department of Applied Physics, University of Zaragoza, 50012 Zaragoza, Spain.
Email: ccar@unizar.es

Funding information
Ministerio de Ciencia e Innovación, Grant/Award Number: RTC-2017-5965-6; BSH Home Appliances Group, Grant/Award Number: -; DGA-FSE, Grant/Award Number: -; Ministerio de Economía, Industria y Competitividad, Gobierno de España, Grant/Award Number: PID2019-103939RB-100

Abstract

Inductive devices are extensively employed in power electronic systems due to their magnetic energy storage and power transfer capabilities. The current trend is towards increasing the frequency of operation in order to reduce the size of the magnetic components, but the main drawback is that the parasitic capacitance effect can become significant, and degrade the performance of the system. This work analyses the influence of this stray capacitance, and considers how to improve the performance of the device. In general, the impact of the stray capacitance on a magnetic component can be reduced by two methods: reducing the parasitic capacitance between turns of the winding or, alternatively, modifying the arrangement of the connection between turns. To evaluate the last option, an approximated expression of the first self-resonant frequency of the magnetic device is proposed. This gives a rapid assessment of the performance of different devices maintaining the overall equivalent inductance. The proposed expression accounts for the influence of the connection between turns in the bandwidth of the component. Finally, some numerical results are verified with planar coils manufactured on two-layer printed circuit boards.

1 | INTRODUCTION

Planar coils are often selected for power electronics systems because these components are well adapted to the geometry of many applications and are convenient for integrated applications. Some examples include inductive power transfer systems (IPTs) [1–7], devices for medical applications [8–12] and domestic induction heating systems [13, 14]. With respect to the integrated applications, there is a tendency towards using planar constructions of inductors and transformers in switching-mode power supplies (SMPS) [15–17]. The most common manufacturing techniques of planar coils are conventional wiring, PCB implementations, as shown in Figure 1, and microfabrication [18].

The present tendency towards higher operation frequencies has also led to an interest in modelling parasitic capacitive effects because, among other reasons, this stray capacitance can be used as the resonant element in converters or determines the bandwidth of the magnetic component. Various proposals trying to capture the capacitive effects by means of equivalent circuits can be found in the literature. One approach is a simple equivalent circuit composed of an equivalent RL circuit connected in parallel to an equivalent capacitance [19]. In other approaches, the value of the frequency-dependent impedance has been obtained by means of empirical methods based on impedance measurements and curve-fitting techniques [20–22].

Although the preceding methods are valuable by themselves, the applicability of the results is limited to the prototypes studied. In these simplified lumped equivalent circuits it is assumed that all turns are driven by the same current and depending on the device or the frequency, the accuracy could be affected and therefore some alternatives have been proposed. These alternatives include distributed circuits [23–29] and transmission line approaches [30], which are mainly focused on obtaining self-resonant frequencies associated with the parasitic capacitances and inductances of the system. These parasitic capacitors could appear, for example, between turns, winding layers or winding and magnetic cores [31–34]. In general, stray capacitances arise from the electrical coupling between elements of the device [35, 36]. However, the connection of the winding's turns can be optimised to improve the bandwidth of the device with a minor impact in its performance [37–41].

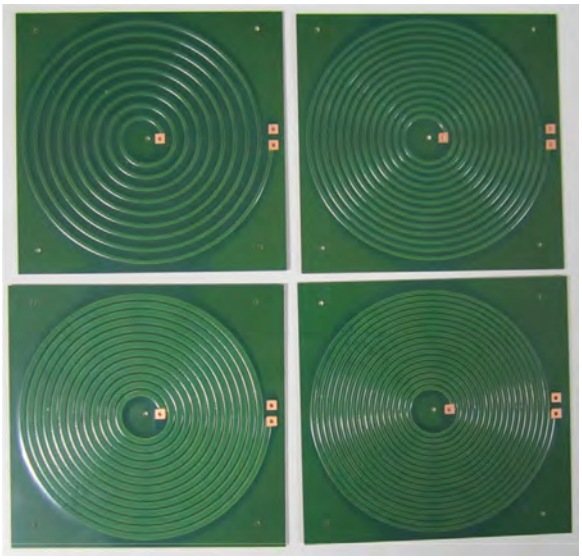

FIGURE 1 Planar PCB coils

In this paper, a simple expression enabling a rapid calculation of the first self-resonant frequency from the distributed circuit elements of the component is derived. In the proposed expression, the circuit elements are intrinsic parameters associated with the geometry and physical properties of the media, but, the first self-resonant frequency is dependent on the turns' arrangement. From this expression it is evident that the bandwidth of the coil can be extended by selecting the appropriate connection between the turns as different connections provide similar low frequency characteristics.

The remainder of the paper is organised as follows: in Section 2, the distributed circuit model for inductors including stray capacitances is described; next, the behaviour of these system are explained in Section 3; in Section 4, the procedure to calculate the distributed circuit element is given; experimental validation of the proposed model is drawn in Section 5 and Section 6 concludes.

2 | ELECTRICAL EQUIVALENT OF THE INDUCTOR

2.1 | Ideal coil

Generally speaking, a planar inductor consists of the series connection of n concentric turns. For the sake of simplicity, spiral turns will be considered in this paper, but the analysis is also valid for turns with alternative geometries, for example, elliptical or square. The turns of a planar coil are placed concentrically to increase the inductance value of the device while maintaining a reduced size. The inductance of this arrangement, L_{eq}, is greater than the sum of the values of the self-inductances of the turns, L_{ii}, due to the effect of the mutual coupling between them, L_{ij}.

Electrical characteristics of an ideal multi-turn coil can be described from the coupling inductances, L_{ij}, which relate the

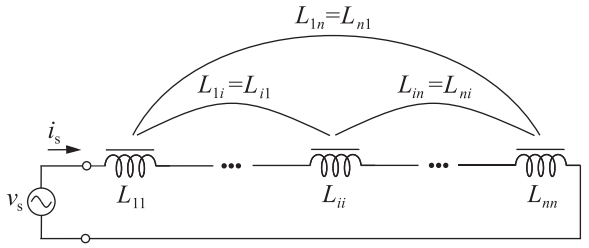

FIGURE 2 Distributed circuit model of an ideal coil

value of the induced voltage V_i in each turn and sources of the magnetic fields, which are given by the current amplitude, I_j, circulating through each turn. In this description, the harmonic approach is assumed, that is, $i_j(t) = \Re e(I_j \cdot e^{j\omega t})$, where ω is the angular frequency of the excitation. The induced voltage in the ith turn, V_i, is determined by the sum of the induced voltages $V_{ij} = L_{ij}I_j$. The induced voltage V_{ij} can be easily carried out by integrating, along the trajectory of the ith turn, the electric field, $\mathbf{E}_j$, created by the current flowing through the jth turn, as stated in [42].

As is commented above, inductors are normally built by connecting the turns in series. Therefore, the current of each turn, I_j, is equal to the source's current, I_S, injected through coil terminals. In that case, the voltage in each turn is therefore $V_i = \sum_{j=1}^{n} j\omega L_{ij} I_S$, and the total voltage in the coil is $V_S = \sum_{i=1}^{n} V_i = j\omega I_S \sum_{i=1}^{n}\sum_{j=1}^{n} L_{ij}$. Thus, the equivalent inductance of the ideal inductor, L_{eq}, is the well-known expression $L_{eq} = \sum_{i=1}^{n}\sum_{j=1}^{n} L_{ij}$, which is independent of the excitation frequency, according to the above assumptions. Moreover, the equivalent inductance, L_{eq}, does not depend on the sequence of the series connection among turns.

Figure 2 represents the circuit diagram of distributed elements corresponding to an ideal winding. Similarly, a circuit of distributed elements can be constructed by dividing the coils into several segments and applying the definition of coupling inductance based on the integration of the electric field along the path of the element. This extended model does not provide additional data but it can be the starting point for a circuit model that includes capacitive effects.

2.2 | Distributed model of the coil with stray capacitances

The model described in the preceding subsection only considers inductive effects arising from currents. However, a complete electrical model of the component also needs to consider the inclusion of capacitive effects. As a consequence, an accurate evaluation of the component considers both self- and coupling inductances as well as stray capacitances, as shown in Figure 3. The stray capacitances are strongly dependent on the geometry and relative distances between segments of the conductors. In particular, multi-layered spiral coils exhibit a highly variable stray capacitance between facing segments of different turns associated with the rapid variation

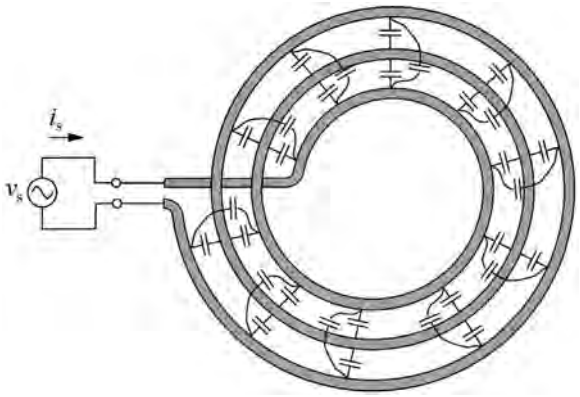

FIGURE 3 Coil with stray capacitances between pair of segments

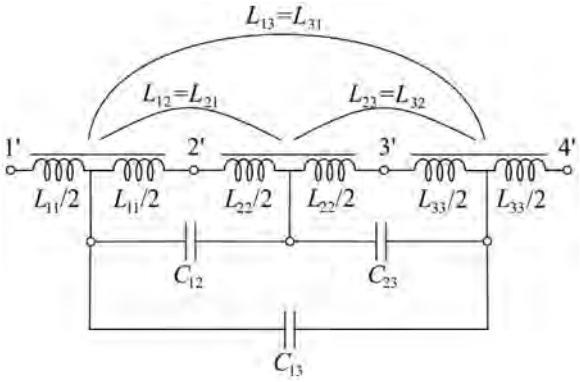

FIGURE 4 Distributed circuit model of a three-turn coil

on their relative positions. Stray capacitances can be found from analytical models [43, 44] as well as from numerical simulations [45–47]. The stray capacitances can also be found by considering segments of conductors at different electric potentials [48].

Stray capacitance can reach high values when the distance between turns is small or facing surfaces are large. In addition, the influence of the dielectric properties of the media, for example substrate of printed circuit boards, play an important role in this characteristic. Stray capacitance provides electrical connection between turns at different voltage levels. The distributed circuit model of an ideal coil depicted in Figure 2 can be easily extended to include capacitive effects by inserting stray capacitances, C_{ij}, connected to the middle points of the ith and jth turns, as shown in Figure 4. As it occurs with the coupling inductances, L_{ij}, the number of stray capacitances depends on the square of the number of turns. However, only parasitic capacitances between nearby turns have a considerable influence in the frequency response of the coil due to the strongly dependence of the stray capacitances with the relative distance between segments of the turns.

The model described in this paper does not consider the effect associated with power losses in the winding, because it would compromise simplicity in describing the behaviour of the system. In order to extend the analysis to include winding losses, on the one hand, it would be necessary to include in the model represented in Figure 4 resistive type elements connected in series with the inductive elements, in order to consider both the current conduction losses and the proximity losses associated with the variable magnetic field in which the conductors are immersed [49, 50]. On the other hand, resistive type elements connected in parallel with the parasitic capacitors should be inserted to model the conduction and dielectric losses in the substrate [51]. However, the preceding elements have a limited impact in the equivalent impedance of the whole system, thus, their influence in the first self-resonant frequency value is moderate.

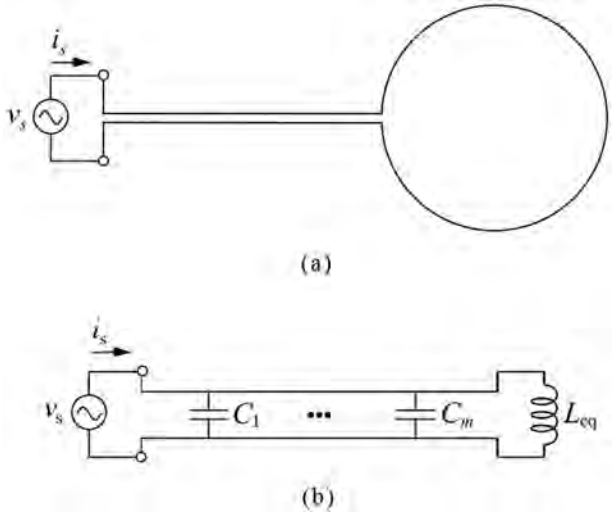

FIGURE 5 Ideal single-turn coil with long terminals. (a) Schematic of the geometry. (b) Distributed element model

3 | ELECTRICAL BEHAVIOUR OF COIL WITH STRAY CAPACITANCES

3.1 | LC-parallel resonant circuit

Stray capacitances in coils introduces additional circuit paths for the current which increase the complexity of analysis of the magnetic device's electrical behaviour. For illustration purposes, a simple reference system composed of a loss-less single-loop coil with long parallel terminals is selected, as shown in Figure 5a. The distributed electrical equivalent of the reference systems is also represented in Figure 5b. As can be seen in the schematic, the equivalent of the single loop is the inductance, L_{eq}, and the long parallel terminals are transformed in parallel-connected stray capacitances, C_i, whose addition provides the equivalent capacitance C_{eq}. At the endpoints of the coil's terminals, a voltage source, $v_S(t)$, is connected driving the current $i_S(t)$. The simplified electrical equivalent of the preceding system is shown in Figure 6a which corresponds to the LC-parallel circuit fed by a voltage source. The current, $i_S(t)$ can be decomposed into two contributions represented in Figure 6b: the capacitor's current or recirculating current, $i_C(t)$, and the inductor's current, $i_L(t)$. Applying the Kirchhoff's current law

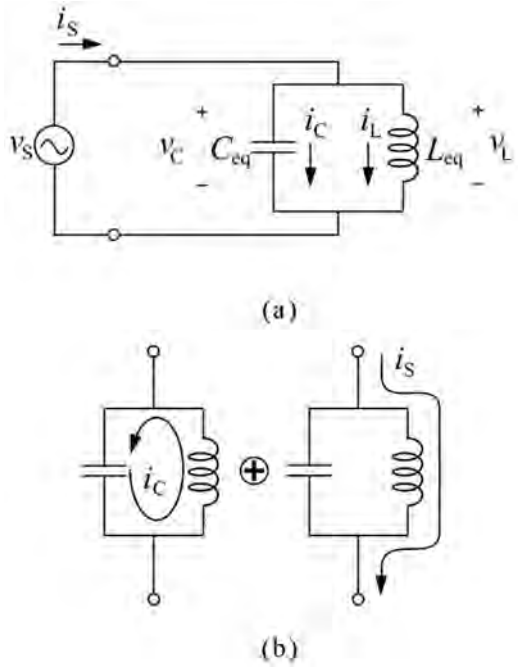

FIGURE 6 Currents in parallel LC resonant tank. (a) Source's current flow. (b) Distributed element model

condition, the relationship $i_S(t) = i_C(t) + i_L(t)$ can be straightforwardly established, and, rearranging the preceding expression, $i_L(t) = i_S(t) - i_C(t)$. Equivalently, the current flowing through the loop turn can also be decomposed into a recirculating current, $i_C(t)$, and a source current $i_S(t)$, as can be seen in Figure 6. Mesh defined by the recirculating current, $i_C(t)$, obeys the Kirchhoff's voltage law, that is, the voltage in the equivalent capacitance, $v_C(t)$, is equal to the voltage in the equivalent inductance, $v_L(t)$. Voltage $v_C(t)$ is totally determined by the product between the recirculating current $i_C(t)$ and the equivalent capacitive impedance, whereas, voltage $v_L(t)$ is given by both the recirculating current, $i_C(t)$, as well as the source current, $i_S(t)$.

At low frequency, the recirculating current is negligible and the current through the equivalent inductance is almost totally equal to the source current, whereas at higher frequencies, the recirculating current increases. Considering the harmonic source's voltage $v_S(t) = V_S e^{j\omega t}$, the recirculating current amplitude is $I_C = j\omega C_{eq} V_S$, and the inductance's current amplitude is $I_L = V_S / j\omega L_{eq}$. The resonant frequency is reached when the inductance's voltage is totally due to the recirculating current, given the source current, $i_S(t)$, equal to zero at this point. The resonant angular frequency is given by the well-known expression $\omega_0 = 1/\sqrt{L_{eq} C_{eq}}$, being infinite the equivalent impedance of the LC-tank circuit.

The preceding LC-tank circuit is selected as the reference system to understand the influence of the parasitic capacitances in *n*-turns coils. Reduction of the distributed circuit model represented in Figure 4 to the concentrated circuit model shown in Figure 6b is a challenging task because the total current carried by each turn is the composition of multiple recirculating currents. As was mentioned, at low frequencies, the recirculating currents are negligible. However, the current distribution changes depending on the turn position when the operation frequency increases. At frequencies close to resonance, the current in the coil is almost totally associated with the recirculating currents. The current reaches its maximum value in the intermediate turns and decays to zero in the turns near the coil terminals. The imaginary part of the current into the terminals is negative or positive, that is inductive or capacitive, respectively, depending on whether the excitation frequency is above or below resonance, respectively.

The resonant frequency of the distributed circuit model will be estimated by weighting the contribution of each parasitic capacitance to the total current in the inductor. At the resonant frequency, the voltage drop between the turns can be determined from the inductive elements' voltages, whereas the effect of the parasitic capacitors comes from the creation of closed paths for the recirculating currents because the current driven by the external voltage source tends to zero at this operating point.

The expression to estimate the first resonance frequency is obtained by performing two different steps: first, the approximate value of the recirculating current can be determined assuming that the same current circulates, I_L through all the turns of the coil as well as recirculating current, $i_{C_{ij}}$ is proportional to the potential drop between the points that present the C_{ij} parasitic capacitance; second, from the recirculation currents, and considering that the current of the source feeding the winding tends to zero at the resonance frequency, that is, the currents in each loop are due to the sum of the recirculation currents, the dependence of the potential drop with respect to the frequency in the complete coil is calculated, being the expression of the approximated self-resonance frequency straightforwardly derived from the preceding relationship.

3.2 | Approximated recirculating currents at resonance

To obtain a simplified expression for the first resonant frequency of a multiple turn coil, the recirculating currents $i_{C_{ij}}$ will be estimated. First, the currents' through the inductive elements at frequencies close to the resonance are approximated to the estimated mean current, $I_i \cong I'_L$. The voltage drop amplitude in the *i*th turn, V_i, can be now given by the following expression:

$$V_i = \sum_{l=1}^{n} j\omega L_{il} I_l \cong j\omega I'_L \sum_{l=1}^{n} L_{il}, \tag{1}$$

where I_l is the current amplitude through the *l*th turn.

The addition of the voltage drop amplitudes over all the turns of the coil gives the total voltage drop in the coil, V_{coil} which is equal to the source's voltage amplitude, V_S:

$$V_S = \sum_{i=1}^{n} V_i \cong j\omega I'_L \sum_{i=1}^{n} \sum_{l=1}^{n} L_{il}. \tag{2}$$

Rewriting the preceding equation, the current amplitude I'_{L} can be approached by the following equation:

$$I'_{\mathrm{L}} \cong \frac{V_{\mathrm{S}}}{j\omega \sum_{i=1}^{n}\sum_{l=1}^{n} L_{il}} = \frac{V_{\mathrm{S}}}{j\omega L_{\mathrm{eq}}}. \tag{3}$$

Similarly, the voltage drop between the middle point $i' + \frac{1}{2}$ of the ith turn and the middle point of the next turn is given by:

$$V_{\left(i'+\frac{1}{2}\right)\left(i'+\frac{1}{2}+1\right)} \cong j\omega I'_{\mathrm{L}}\left(\sum_{l=1}^{n}\frac{L_{il}}{2} + \sum_{l=1}^{n}\frac{L_{(i+1)l}}{2}\right). \tag{4}$$

And the voltage drop between the terminals of the parasitic capacitor, $V_{C_{ij}} = V_{(i'+\frac{1}{2})(j'+\frac{1}{2})}$, can be approached by:

$$V_{C_{ij}} \cong j\omega I'_{\mathrm{L}} \sum_{m=i}^{j-1}\left(\sum_{l=1}^{n}\frac{L_{ml}}{2} + \sum_{l=1}^{n}\frac{L_{(m+1)l}}{2}\right). \tag{5}$$

Substituting the value I'_{L} given by (3), we obtain:

$$V_{C_{ij}} \cong \sum_{m=i}^{j-1}\sum_{l=1}^{n}\frac{L_{ml} + L_{(m+1)l}}{2L_{\mathrm{eq}}} V_{\mathrm{S}}. \tag{6}$$

The last expression establishes the relationship between the voltage drop, $V_{C_{ij}}$, in the middle points of the ith and jth turns, respectively, and the source's voltage, V_{S}. To a certain extent, expression (6) could be considered as the formula of a voltage divider. The factor of proportionality, $F_{C_{ij}}$, defined from the identity $V_{C_{ij}} = F_{C_{ij}} V_{\mathrm{S}}$, can be expressed as:

$$F_{C_{ij}} = \sum_{m=i}^{j-1}\sum_{l=1}^{n}\frac{L_{ml} + L_{(m+1)l}}{2L_{\mathrm{eq}}}. \tag{7}$$

The factor of proportionality, $F_{C_{ij}}$, ranges from 0 to 1, because it is positively defined and the maximum value is reached for the middle points of the turns connected to the coil's terminals. For the maximum value configuration, the voltage drop $V_{C_{1n}}$ is lower to V_{S} due to the non-zero voltage drops between the coil's terminals and the middle points of the extreme turns, $V_{1'(1+\frac{1}{2})'}$ and $V_{(n+\frac{1}{2})'(n+1)'}$, respectively. The factor of proportionality, $F_{C_{ij}}$, is independent of the frequency, as it also occurs for the stray capacitances, but presents dependence on the self- and mutual inductances of the turns, that is, it depends on the geometry and magnetic properties of the coil. Note that the factor of proportionality, $F_{C_{ij}}$, can be modified by changing the arrangement of connections between turns but the equivalent inductance of the coil, L_{eq}, remains the same. Equation (6) can be rewritten as:

$$V_{C_{ij}} \cong F_{C_{ij}} V_{\mathrm{S}}. \tag{8}$$

Capacitive recirculating current $I_{C_{ij}}$ is proportional to the voltage drop between the stray capacitor terminals placed in the middle points of the ith and jth turns, as it is given by $I_{C_{ij}} = j\omega C_{ij} V_{C_{ij}}$. Thus, considering Equation (8), the recirculating current $I_{C_{ij}}$ can be expressed as:

$$I_{C_{ij}} \cong j\omega F_{C_{ij}} C_{ij} V_{\mathrm{S}}. \tag{9}$$

By defining the frequency-independent corrected capacitance between the ith and jth turns, C^*_{ij}, as:

$$C^*_{ij} = F_{C_{ij}} C_{ij}. \tag{10}$$

Thus, the recirculating current amplitude can be rewritten as:

$$I_{C_{ij}} \cong j\omega C^*_{ij} V_{\mathrm{S}}. \tag{11}$$

As can be appreciated in the preceding expression, the corrected capacitance C^*_{ij} represents the effective capacitance associated with the stray capacitance. As a consequence, the influence of the physical stray capacitance can be altered by modifying the factor of proportionality, $F_{C_{ij}}$, that is. changing the turns between terminals of the stray capacitance.

3.3 | Approximated first self-resonant frequency

Once the recirculating current amplitude is estimated, the overall current carried by the inductive elements of the distributed model at resonance can be calculated by the addition of the recirculating currents because the source's current is zero at this operating point. The estimated current, $I'_{i'+1}$, at resonance through the $i' + 1$th point is:

$$I'_{i'+1} \cong \sum_{k=1}^{i'}\sum_{m=i'+1}^{n} -I_{C_{km}}, \tag{12}$$

which corresponds to the current flowing through inductance element with terminals at the $i' + \frac{1}{2}$th and $i' + 1$th endpoints as well as the element at the $i' + 1$th and $i' + \frac{1}{2} + 1$th endpoints. The estimated voltage drop in the ith turn, V'_i, can be calculated as:

$$V'_i \cong j\omega_0\left(\sum_{l=1}^{n-1}\frac{L_{il}}{2} I'_{(l+1)'} + \sum_{l=1}^{n-1}\frac{L_{i(l+1)}}{2} I'_{(l+1)'}\right). \tag{13}$$

Including (12) in the preceding expression, yields:

$$V'_i \cong -j\omega_0 \sum_{l=1}^{n-1}\sum_{k=1}^{l}\sum_{m=l+1}^{n}\frac{L_{il} + L_{i(l+1)}}{2} I_{C_{km}}. \tag{14}$$

Thus, the total voltage amplitude in the coil is the addition of the voltages' amplitudes, V'_i over all the turns:

$$V'_{\text{coil}} \cong -j\omega_0 \sum_{i=1}^{n} \sum_{l=1}^{n-1} \sum_{k=1}^{l} \sum_{m=l+1}^{n} \frac{L_{il} + L_{i(l+1)}}{2} I_{C_{km}}. \quad (15)$$

The coil's voltage amplitude is $V_S = V'_{\text{coil}}$, and the recirculating current is given by (11), thus:

$$V_S \cong \omega_0^2 \sum_{i=1}^{n} \sum_{l=1}^{n-1} \sum_{k=1}^{l} \sum_{m=l+1}^{n} \frac{L_{il} + L_{i(l+1)}}{2} C^*_{km} V_S. \quad (16)$$

Rearranging the preceding expression:

$$\omega_0^2 \cong \frac{V_S}{\sum_{i=1}^{n} \sum_{l=1}^{n-1} \sum_{k=1}^{l} \sum_{m=l+1}^{n} \frac{L_{il}+L_{i(l+1)}}{2} C^*_{km} V_S}. \quad (17)$$

And, finally, the first self-resonant angular frequency can be approximated by the following relationship:

$$\omega_0 \cong \frac{1}{\sqrt{\sum_{i=1}^{n} \sum_{l=1}^{n-1} \sum_{k=1}^{i} \sum_{m=i+1}^{n} \frac{L_{il}+L_{i(l+1)}}{2} C^*_{km}}}. \quad (18)$$

Equation (18) can also lead to an estimation of the parallel resonant capacitor of the lumped circuit equivalent shown in Figure 6a. From the definition, $\omega_0 = 1/\sqrt{L_{\text{eq}} C_{\text{eq}}}$, the equivalent capacitance is provided by:

$$C_{\text{eq}} \cong \sum_{i=1}^{n} \sum_{l=1}^{n-1} \sum_{k=1}^{l} \sum_{m=l+1}^{n} \frac{L_{il} + L_{i(l+1)}}{2L_{\text{eq}}} C^*_{km}. \quad (19)$$

This means that ω_0 can be increased by reducing the equivalent capacitance applying the correct arrangement of the turns which is useful because it increases the bandwidth of the inductive device.

4 | CALCULATION OF THE DISTRIBUTED CIRCUIT ELEMENTS

4.1 | Inductive parameters

The analytical expression of the inductance for a coil made of filiform concentric spiral loops is already found in Maxwell's treatise [52]. Despite, analytical expressions for alternative inductor structures are not easily available, the self- and mutual inductance assuming linear conditions can be easily calculated with numerical tools. Simplified geometric structures provide accurate results due to the low sensitivity of the mutual coupling between turns. Consequently, mutual inductance can be calculated by taking advantage of an imperfect symmetry, as it occurs for spiral winding which can be accurately modelled with 2D axisymmetric models. Inductive elements, L_{ij}, can be easily extracted from the relationship between the induced voltage in the jth turn, V_j, and the current amplitude, I_i through the ith turn, as is given in [42].

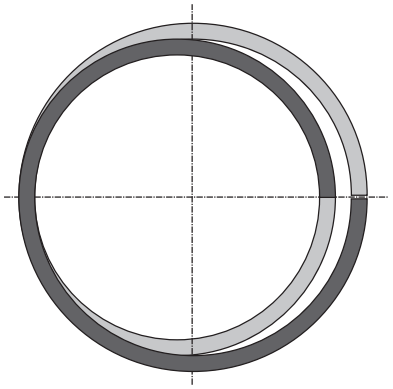

FIGURE 7 Two series-connected spiral turns placed in parallel planes (dark grey: upper layer turn, light grey: lower layer turn) connected in the inner radius common point

4.2 | Capacitive parameters

The total capacitance between two turns corresponds to the total effect of several distributed capacitances. Stray capacitances can be also evaluated from analytical expressions in simplified structures [53], but analytical expressions are not available for common arrangements or are inaccurate [54]. However, the numerical extraction of the parasitic capacitances can be performed in an easy way because they are physically decoupled from the inductive effects. Parasitic capacitance C_{ij} can be calculated by addition of the capacitance for facing segments of the turns. The numerical extraction of stray capacitance can be performed by applying $C_{ij} = Q_j/V_i$, where Q_j is the charge accumulated in the jth turn when a voltage V_i is applied in the i turn, and the remaining turns grounded.

4.3 | Example of parameter calculation

The electrical parameter extraction of the two-turn coil represented in Figure 7 is performed with COMSOL®. Computational extraction can determine both inductive and capacitive elements of the device [55, 56]. Turns are built of standard PCB copper tracks with thickness, $h = 70$ μm, and width, $w = 500$ μm, placed in each side of the board with thickness, $t = 1.55$ mm, respectively. The middle points of the internal terminals are at radial distance, $r_{\text{int}} = 30$ mm, and the external terminals are at $r_{\text{ext}} = 31$ mm, that is, the separation between tracks is $d = 500$ μm. Self- and mutual inductances can be easily calculated

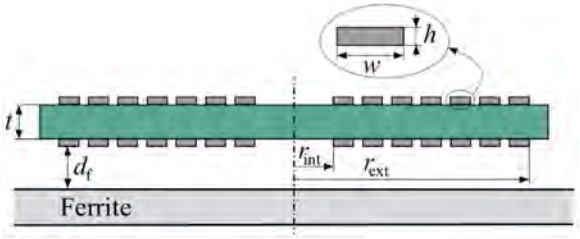

FIGURE 8 Schematic of the PCB-coil (side view including axis of revolution)

by using the magneto-quasi-static approach. Turns are modelled by two rectangular cross-section turns with axial 2D symmetry of mean radius $r_i = r_j = 30.5$ mm facing at a distance t. Magnetic field arises from the current I_i uniformly distributed in the cross-section area of the ith turn. The induced voltages V_i and V_j of the ith and jth turns have been derived by integrating the electric field. Finally, self-inductance, $L_{ii} = 211$ nH, and mutual inductance $L_{ij} = 115$ nH, are obtained from numerical simulations, respectively, being a good approach of the exact values. In case of inserting magnetic materials, parameter extraction can be performed in a similar fashion because numerical tools easily include the influence of these elements by considering an object with a high relative permeability.

On the other hand, stray capacitance, C_{ij}, was obtained by applying the electro-quasi-static approach, because the frequency dependence of the capacitance associated with the skin effect can be neglected for conductors of small cross-sectional area, as it occurs in the coils analysed in this work. The dielectric constant of the FR4 substrate is $\epsilon_r = 5$. First, the turns are divided into N angular segments. Partial axial symmetry is exploited for each pair of facing segments, but can be also considered as straight segments with a similar outcome. Partial parasitic capacitances ranges from 1.04 to 1.20 pF per radian, due to the variation of the distance between segments with respect to the angular position. The calculated two-turn stray capacitance is $C_{ij} = 7.18$ pF.

5 | EXPERIMENTAL RESULTS

Three prototypes of two-layer PCB coils with $n = 30$ equally distributed turns were built to validate the numerical values using standard copper thickness, $h = 70$ μm, and dielectric thickness, $t = 1.55$ mm, of FR4 material ($\epsilon_r = 5$). The remaining common characteristics of the prototypes, as shown in Figure 8, are the following: external radius, $r_{ext} = 60$ mm, internal radius, $r_{int} = 30$ mm, and trace width, $w = 500$ μm, respectively. Furthermore, a distance from the coil to the ferrite equal to $d_f = 1$ mm was set. The first and the second prototypes were tested with terminals placed at different turns, but in both cases the connection is performed from outer turn to inner turn in the bottom layer and in the opposing sense for the top layer. The first configuration is defined by the coil's terminals placed at outer turns, that is first and nth turns, as can be seen in Figure 9a, and the second one corresponds to the terminals

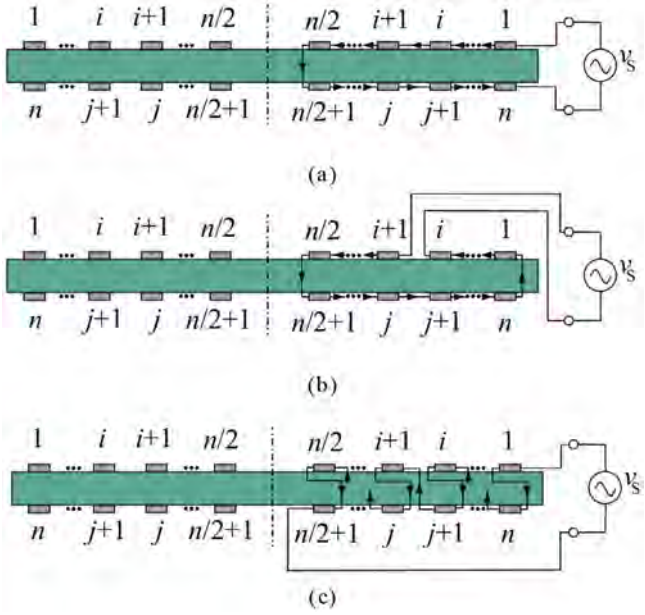

FIGURE 9 Reference winding arrangements of n-turns (side view including axis of revolution): (a) outer connection; (b) intermediate connection; (c) alternating-layers connection

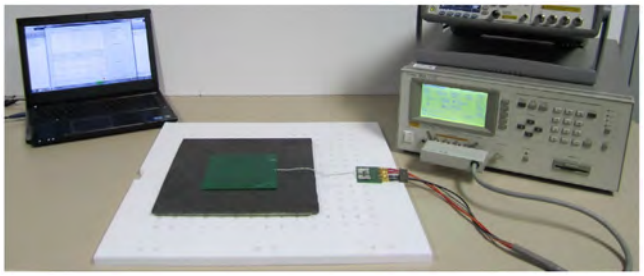

FIGURE 10 Experimental set-up for measuring PCB coil with ferrite

at seventh and eighth turns of the top layers, as shown in Figure 9b. In addition, the last prototype was built by series connecting the turns from outer-to-inner radius turns, but, sequentially exchanging the layer by means of n-1 vias. Measurements were performed with a high precision LCR-meter HP 4285A (measurement frequencies range from 75 kHz to 30 MHz and the basic accuracy of the measurements is 0.1 %), as shown in Figure 10.

Figure 11a shows the reactance-to-angular frequency ratio, equivalent to the inductance at low frequencies, for the coil in air configurations. Model-based values are calculated from the same distributed circuit parameters, thus, the equivalent inductance of both configurations are the same but the equivalent capacitance differs because different corrected capacitances are obtained. The change in the values of the corrected capacitances for each configuration is due to the variation in the values of the proportionality factors, $F_{C_{ij}}$, defined in (7) because the parasitic capacity between the ith and the jth turns, C_{ij}, remain constant in all configurations. Therefore, when applying a different connection of the turns, the equivalent capacitance, C_{eq} can be

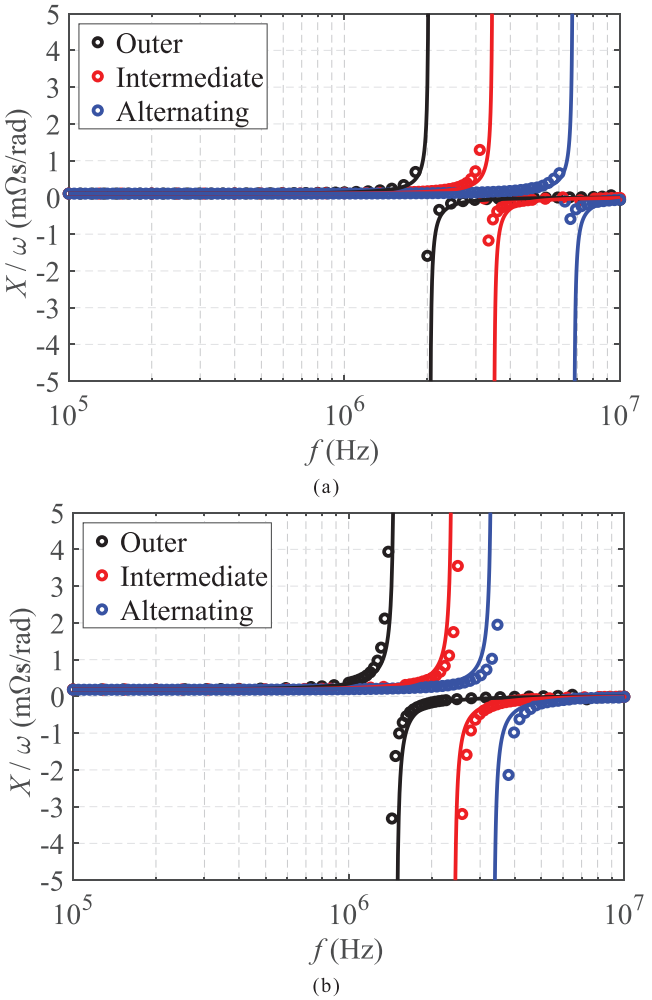

FIGURE 11 Ratio between reactance and angular frequency experimental (circles) and model-based (solid lines) values applying the outer (black) and intermediate (red) connection-modes. (a) Two-layer PCB coil in air. (b) Two-layer PCB coil with ferrite

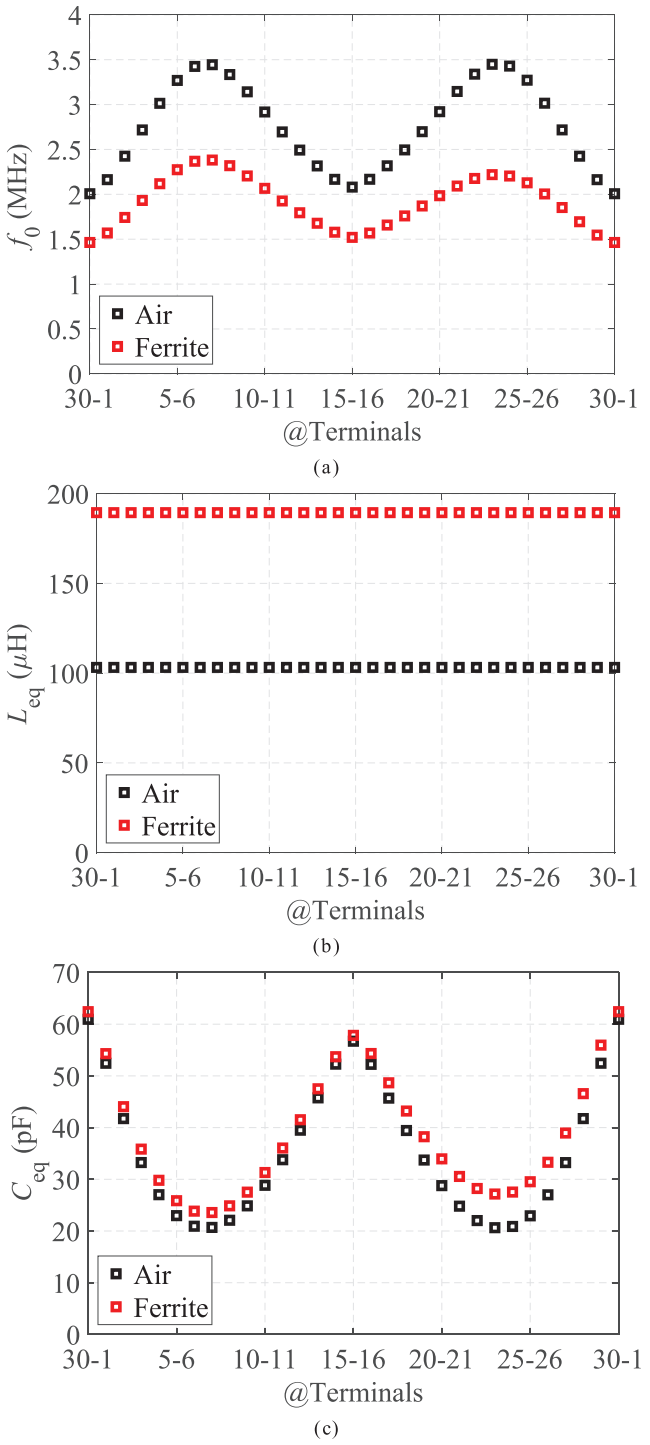

FIGURE 12 Numerical results for coil's terminals at different consecutive positions (black: coil in air, red: coil with ferrite plane). (a) First self-resonant frequency, f_0. (b) Equivalent inductance, L_{eq}. (c) Equivalent capacitance, C_{eq}

reduced if the configuration reduces the proportionality factors, $F_{C_{ij}}$, between the turns with the highest parasitic capacitance between them. Moreover, Figure 11b shows the results when a ferrite layer of magnetic permeability, $\mu_{r,f} = 2000$, is inserted at a distance of $d_f = 1$ mm below the coil, with a good agreement between experimental and modelled data because the mismatch between them arise from a slight difference on the first self-resonant frequencies in the prototype and the simulation results but a high correlation in the frequency dependence between both types of values is observed for the different configurations. As can be seen in the graphs, configurations with the intermediate turns' terminals extend the bandwidth of the coil compared to configurations with the outer turns' terminals but better results are achieved when facing turns located at different layers are connected between them, as it occurs in the last prototype. However, the construction of the last configuration exhibits two main drawbacks: including vias in the coil would impact in the power losses in the coil and the terminal are placed into distant points. A comparison between the simulated values and the measured first resonant frequencies for the tested arrangements is given in Table 1. Experimental first self-resonant frequencies, f_0, are obtained by fitting the measured impedances to the frequency response of parallel LC resonant tanks.

Figure 12 presents the expected first self-resonant frequency calculated for the equivalent inductance, L_{eq} and equivalent

TABLE 1 Self-resonant frequency and electrical parameters of 30-turn coil

Additional media	Connection mode	Measured parameters			Simulated parameters		
		f_0 (MHz)	L_{eq} (μH)	C_{eq} (pF)	f_0 (MHz)	L_{eq} (μH)	C_{eq} (pF)
Air	Outer turns	2.09	103.84	55.84	2.01	103.19	60.75
	Intermediate turns	3.21	103.84	23.64	3.44	103.19	20.74
	Alternating turns	6.31	102.70	6.19	6.77	103.19	5.36
Ferrite plane	Outer turns	1.44	189.30	64.89	1.48	189.20	61.30
	Intermediate turns	2.54	187.40	21.03	2.39	189.20	23.36
	Alternating turns	3.63	180.90	10.60	3.33	189.20	12.07

TABLE 2 Self-resonant frequency of two-layer PCB coil

Turns	Measured f_0 (MHz)	Simulated f_0 (MHz)
18	6.17	5.70
26	3.61	3.43
34	2.56	2.47

capacitance, C_{eq} of the tested arrangements but varying the position of the coil's terminals, starting from the outer connection, that is 1st and 30th turns, and varying the connection sequentially. Outer connection and inner connection exhibit a similar performance because turns with large stray capacitances are connected through a high number of intermediate turns, implying a high value of corrected stray capacitances. Maximum self-resonant frequency is achieved for coils with terminals at intermediate turns, but the upper-layer connection is weakly preferred for the coil with ferrite plane. Alternative complex connections can increase the bandwidth of the inductor, that is, first, up-to-down or down-to-up turns' connection and, next, outer-to-inner connection gives resonant frequencies at $f_0 = 6.77$ MHz for coil in air and $f_0 = 3.33$ MHz for coil with ferrite plane. As can be seen in Figure 12c, the equivalent capacitance is clearly dependent on the arrangement of the turns, but the inclusion of the ferrite plane slightly increases its value.

Additionally, three prototypes of two-layer PCB coils with $n = 18$, $n = 26$ and $n = 34$ equally distributed turns were also built using copper thickness, $h = 400$ μm, and dielectric thickness, $t = 1.55$ mm, of FR4 material ($\epsilon_r = 5$). The remaining common characteristics of the prototypes are the following: external radius, $r_{ext} = 60$ mm, internal radius, $r_{int} = 12$ mm, and trace width, $w = 2000$ μm, respectively. A comparison between the measurement data and the model results are shown in Figure 13, and the self-resonant frequency extracted from the measurements and the calculated self-resonant frequency, f_0, are listed in Table 2 wherethe good agreement between them can be seen. Calculated self-resonant frequencies are obtained from self-inductances of 18.20, 38.01 and 65.21 μH, and corrected capacitances of 42.82, 56.57 and 65.54 pF, respectively.

Finally, an arrangement composed of two PCB's was made to double the number of turns by applying a series connection between them in order to test the proposed model for multi-layered coil configurations. The new configuration was built by using two PCBs with the same characteristic of the preceding arrangement. The distance between PCB's in that case is fixed to 1.55 mm. These configurations verify the generality of the proposed model. In that case, the comparison between the experimental and model results are shown in Figure 14 verifying the correctness of the proposed model because, as can be seen

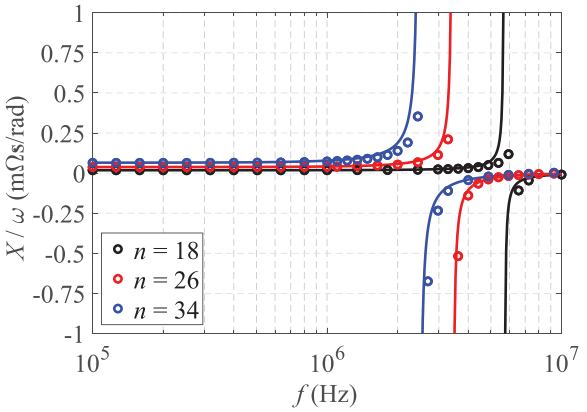

FIGURE 13 Ratio between reactance and angular frequency experimental measurements (circular symbols) and model-based values (solid lines) for two-layer PCB coils of $n = 18$ turns, $n = 26$ turns and $n = 34$ turns

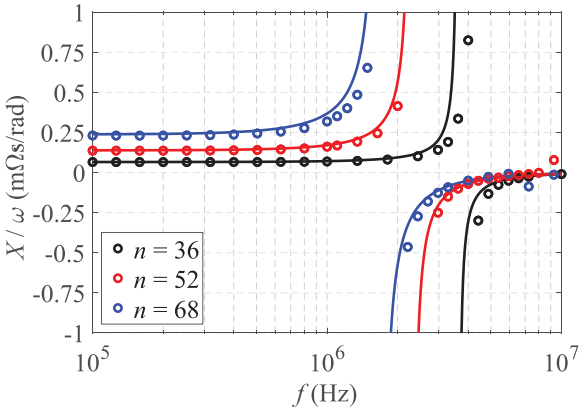

FIGURE 14 Ratio between reactance and angular frequency experimental measurements (circular symbols) and model-based values (solid lines) for four-layer PCB coils of $n = 36$ turns, $n = 52$ turns and $n = 68$ turns

TABLE 3 Self-resonant frequency of four-layer PCB coil by stacking two two-layer PCBs

Turns	Measured f_0 (MHz)	Simulated f_0 (MHz)
36	3.98	3.62
52	2.44	2.30
68	1.75	1.68

in Table 3, the accuracy of the estimated self-resonant frequency is about 10% which can be considered adequate for this kind of approach. Calculated self-resonant frequencies are obtained from self-inductances of 65.91, 138.35 and 237.80 μH, and corrected capacitances of 29.21, 34.57 and 37.63 pF, respectively. It should be noted that the corrected capacitances in the two PCB's configurations are lower than the corrected capacitances of the single PCB configurations because the gap between PCB's, which is similar to the thickness of a PCB, is filled with a lower permittivity material than FR-4, that is air, which reduces parasitic capacitances, and, particularly, the fraction of the input voltage between facing segments is reduced when two PCB's are connected in series. As a result, factor $F_{C_{ij}}$ decreases, and, consequently, the corrected capacitance in (10) is also reduced. Without loss of generality, the results shown in the latter configurations validate the proposed analysis for multi-layered coils with turns placed in three or more parallel planes.

6 | CONCLUSION

In this paper, the influence of stray capacitances in magnetic devices is analysed with the purpose of building extended bandwidth inductors. As a result of the analysis, an approximated expression for the first self-resonance frequency is derived for evaluating its impact on the performance of the device. The application of the correct arrangement of the turns in an inductor can extend the frequency bandwidth of the device with no influence in the value of the equivalent inductance. This effect was reported in the past, but in this work, both a physical interpretation and an analytical expression are provided. The proposed expression to estimate the first self-resonance frequency enables a rapid procedure to carry out the values for difference configurations after evaluating the distributed parameters of the inductor. Multi-layered coils are not included in the experimental validation but the analysis can be easily extended to this structure with no additional effort.

The outcome of this work shows that the distributed circuit elements only depend on the sizes and location of the turns as well as physical properties, that is, magnetic permeability, electrical conductivity and dielectric permittivity, of system media, which are frequency independent over a wide range, contrary to the equivalent impedance of the system. However, the corrected parasitic capacitances also depend on the physical connection of the turns. Among other options, the resonant frequency for a certain arrangement of turns can be modified by changing the position of the inductor terminals connected to the voltage source with a negligible effect on the equivalent inductance at frequency below the first self-resonance.

The proposed method for calculating the first self-resonance frequency of the arrangement of the different turns of the coil provides a rapid method for optimising the configuration of the coil, because it provides a figure of merit based on simulation results. Alternatively, measurement-based optimisation methods could be used using an impedance analyser, but have the disadvantage of requiring prototypes with the different coil configurations to be characterised, which can be costly to build in both time and effort.

Finally, as a rule of thumb, a pair of turns with a high stray capacitance, that is, facing tracks, should have a low number of turns between them in order to reduce the corrected capacitance between turns, whereas turns with a low mutual stray capacitance can be connected far away.

ACKNOWLEDGEMENTS

This work was partly supported by the Spanish MINECO under Project PID2019-103939RB-100, by the Spanish MICINN and AEI under Project RTC-2017-5965-6, by the BSH Home Appliances Group and by the DGA-FSE.

ORCID

Claudio Carretero https://orcid.org/0000-0001-7901-9174

REFERENCES

1. Choi, B.H., et al.: Lumped impedance transformers for compact and robust coupled magnetic resonance systems. IEEE Trans. Power Electron. 30(11), 6046–6056(2015)
2. Kim, J.H., et al.: Plane type receiving coil with minimum number of coils for omnidirectional wireless power transfer. IEEE Trans. Power Electron. 35(6), 6165–6174(2020)
3. Li, Z., et al.: Design of coils on printed circuit board for inductive power transfer system. IET Power Electron. 11(15), 2515–2522 (2018)
4. Jeong, S., et al.: Smartwatch strap wireless power transfer system with flexible pcb coil and shielding material. IEEE Trans. Ind. Electron. 66(5), 4054–4064(2019)
5. Acero, J., et al.: Analysis of the mutual inductance of planar-lumped inductive power transfer systems. IEEE Trans. Ind. Electron. 60(1), 410–420(2013)
6. Hsieh, Y., et al.: High-efficiency wireless power transfer system for electric vehicle applications. IEEE Trans. Circuits Syst. II 64(8), 942–946 (2017)
7. Aziz, A.F.A., et al.: Review of inductively coupled power transfer for electric vehicle charging. IET Power Electron. 12(14), 3611–3623(2019)
8. Felic, G.K., et al.: Investigation of frequency-dependent effects in inductive coils for implantable electronics. IEEE Trans. Magn. 49(4), 1353–1360(2013)
9. Xue, R., et al.: High-efficiency wireless power transfer for biomedical implants by optimal resonant load transformation. IEEE Trans. Circuits Syst. I 60(4), 867–874(2013)
10. Ha-Van, N., Seo, C.: Modeling and experimental validation of a butterfly shaped wireless power transfer in biomedical implants. IEEE Access 7, 107225–107233(2019)
11. Knecht, O., et al.: High-efficiency transcutaneous energy transfer for implantable mechanical heart support systems. IEEE Trans. Power Electron. 30(11), 6221–6236(2015)
12. Ghovanloo, M., Atluri, S.: A wide-band power-efficient inductive wireless link for implantable microelectronic devices using multiple carriers. IEEE Trans. Circuits Syst. I 54(10), 2211–2221(2007)

13. Lope, I., et al.: Design and implementation of PCB inductors with litz-wire structure for conventional-size large-signal domestic induction heating applications. IEEE Trans. Ind. Appl. 51(3), 2434–2442 (2015)
14. Serrano, J., et al.: A flexible cooking zone composed of partially overlapped inductors. IEEE Trans. Ind. Electron. 65(10), 7762–7771 (2018)
15. Andersen, T.M., et al.: Modeling and Pareto optimization of microfabricated inductors for power supply on chip. IEEE Trans. Power Electron. 28(9), 4422–4430(2013)
16. Ouyang, Z., Andersen, M.A.E.: Overview of planar magnetic technology—Fundamental properties. IEEE Trans. Power Electron. 29(9), 4888–4900(2014)
17. Zhang, J., et al.: Leakage inductance calculation for planar transformers with a magnetic shunt. IEEE Trans. Ind. Appl. 50(6), 4107–4112 (2014)
18. Feeney, C., et al.: Design procedure for racetrack microinductors on silicon in multi-MHz DC-DC converters. IEEE Trans. Power Electron. 30(12), 6897–6905(2015)
19. Hurley, W.G., Duffy, M.C.: Calculation of self and mutual impedances in planar magnetic structures. IEEE Trans. Magn. 31(4), 2416–2422 (1995)
20. Kotny, J.L., et al.: High-frequency model of the coupled inductors used in EMI filters. IEEE Trans. Power Electron. 27(6), 2805–2812 (2012)
21. Tan, W., et al.: A high frequency equivalent circuit and parameter extraction procedure for common mode choke in the EMI filter. IEEE Trans. Power Electron. 28(3), 1157–1166(2013)
22. Wojda, R.P., Kazimierczuk, M.K.: Winding resistance of litz-wire and multi-strand inductors. IET Power Electron. 5(2), 257–268(2012)
23. Dehui, W., et al.: Method for the calculation of coupling coefficient between two arbitrary-shaped coils. IET Power Electron. 12(15), 3936–3941(2019)
24. Chen, K., Zhao, Z.: Analysis of the double-layer printed spiral coil for wireless power transfer. IEEE J. Emerging Sel. Top. Power Electron. 1(2), 114–121(2013)
25. Kovacic, M., et al.: Analytical wideband model of a common-mode choke. IEEE Trans. Power Electron. 27(7), 3173–3185(2012)
26. Yang, Q., et al.: Distributed capacitance effects on the transmission performance of contactless power transfer for rotary ultrasonic grinding. IET Power Electron. 11(3), 548–556(2018)
27. Niknejad, A.M., Meyer, R.G.: Analysis, design, and optimization of spiral inductors and transformers for Si RF ICs. IEEE J. Solid-State Circuits 33(10), 1470–1481(1998)
28. Pon, L.L., et al.: Displacement tolerant printed spiral resonator with capacitive compensated plates for non radiative wireless energy transfer. IEEE Access 7, 10037–10044(2019)
29. Pon, L.L., et al.: Printed spiral resonator for displacement tolerant near-field wireless energy transfer. IEEE Access 7, 172055–172064(2019)
30. Breitkreutz, B., Henke, H.: Calculation of self-resonant spiral coils for wireless power transfer systems with a transmission line approach. IEEE Trans. Magn. 49(9), 5035–5042(2013)
31. Chan, P.C.F., et al.: Stray capacitance calculation of coreless planar transformers including fringing effects. Electron. Lett. 43(23), (2007)
32. Miranda, C.M.d., Pichorim, S.F.: A self-resonant two-coil wireless power transfer system using open bifilar coils. IEEE Trans. Circuits Syst. II 64(6), 615–619(2017)
33. Hole, M.J., Appel, L.C.: Stray capacitance of a two-layer air-cored inductor. IEE Proceedings Circuits, Devices and Systems 152(6), 565–572 (2005)
34. Massarini, A., Kazimierczuk, M.K.: Self-capacitance of inductors. IEEE Trans. Power Electron. 12(4), 671–676(1997)
35. Fouda, M.E., et al.: Modeling and analysis of passive switching crossbar arrays. IEEE Trans. Circuits Syst. I 65(1), 270–282(2018)
36. Guan, Y., et al.: A high-frequency CLCL converter based on leakage inductance and variable width winding planar magnetics. IEEE Trans. Ind. Electron. 65(1), 280–290(2018)
37. Ghotbi, I., et al.: Enhanced power-delivered-to-load through planar multiple-harmonic wireless power transmission. IEEE Trans. Circuits Syst. II 65(9), 1219–1223(2018)
38. Xie, L., et al.: Reducing common mode noise in phase-shifted full-bridge converter. IEEE Trans. Ind. Electron. 65(10), 7866–7877(2018)
39. Yammouch, T., et al.: Physical modeling of MEMS variable inductor. IEEE Trans. Circuits Syst. II 55(5), 419–422(2008)
40. Lee, C.K., et al.: Printed spiral winding inductor with wide frequency bandwidth. IEEE Trans. Power Electron. 26(10), 2936–2945(2011)
41. Pahlevaninezhad, M., et al.: An improved layout strategy for common-mode EMI suppression applicable to high-frequency planar transformers in high-power DC/DC converters used for electric vehicles. IEEE Trans. Power Electron. 29(3), 1211–1228(2014)
42. Carretero, C., et al.: Coupling impedance between planar coils inside a layered media. Progress Electromagnetics Research 112, 381–396(2011)
43. Ayachit, A., Kazimierczuk, M.K.: Self-capacitance of single-layer inductors with separation between conductor turns. IEEE Trans. Electromagn. Compat. 59(5), 1642–1645(2017)
44. Pasko, S.W., et al.: Self-capacitance of coupled toroidal inductors for EMI filters. IEEE Trans. Electromagn. Compat. 57(2), 216–223(2015)
45. Qin, Y., Holmes, T.W.: A study on stray capacitance modeling of inductors by using the finite element method. IEEE Trans. Electromagn. Compat. 43(1), 88–93(2001)
46. Greve, Z.D., et al.: Numerical modeling of capacitive effects in HF multiwinding transformers, Part I: A rigorous formalism based on the electrostatic equations. IEEE Trans. Magn. 49(5), 2017–2020 (2013)
47. Greve, Z.D., et al.: Numerical modeling of capacitive effects in HF multiwinding transformers, Part II: Identification using the finite-element method. IEEE Trans. Magn. 49(5), 2021–2024 (2013)
48. Biela, J., Kolar, J.W.: Using transformer parasitics for resonant converters—A review of the calculation of the stray capacitance of transformers. IEEE Trans. Ind. Appl. 44(1), 223–233(2008)
49. Phung, A., et al.: High-frequency proximity losses determination for rectangular cross-section conductors. IEEE Trans. Magn. 43(4), 1213–1216(2007)
50. Lope, I., et al.: Ac power losses model for planar windings with rectangular cross-sectional conductors. IEEE Trans. Power Electron. 29(1), 23–28(2014)
51. Hjellen, G.A.: Including dielectric loss in printed circuit models for improved EMI/EMC predictions. IEEE Trans. Electromagn. Compat. 39(3), 236–246(1997)
52. Maxwell, J.C.: A Treatise on Electricity and Magnetism. Clarendon press, Oxford (1873)
53. Fu, D., et al.: Novel techniques to suppress the common-mode EMI noise caused by transformer parasitic capacitances in dc-dc converters. IEEE Trans. Ind. Electron. 60(11), 4968–4977(2013)
54. Aghaei, M., Kaboli, S.: On the effect of disorder on stray capacitance of transformer winding in high-voltage power supplies. IEEE Trans. Ind. Electron. 64(5), 3608–3618(2017)
55. Zhao, B., et al.: An improved partially interleaved transformer structure for high-voltage high-frequency multiple-output applications. In: IECON 2017-43rd Annual Conference of the IEEE Industrial Electronics Society, pp. 798–804 (2017)
56. Cove, S.R., et al.: Applying response surface methodology to small planar transformer winding design. IEEE Trans. Ind. Electron. 60(2), 483–493(2013)

How to cite this article: Lope I, Carretero C, Acero J. First self-resonant frequency of power inductors based on approximated corrected stray capacitances. *IET Power Electron.* 2021;14:257–267.
https://doi.org/10.1049/pel2.12030